

Temporal fluctuation and its power law in the crystalline-to-glass transition during electron irradiation

S. WATANABE[†], M. HOSHINO, T. KOIKE[‡], T. SUDA, S. OHNUKI

Division of Materials Science, Graduate School of Engineering,
Hokkaido University, Kita-13, Nishi-8, Kita-ku, Sapporo 060-8628, Japan

H. TAKAHASHI

Center for Advanced Research of Energy Technology, Hokkaido University,
Kita-13, Nishi-8, Kita-ku, Sapporo 060-8628, Japan

and N. Q. LAM

Materials Science Division, Argonne National Laboratory, Argonne,
Illinois 60439, USA

[Received 25 October 2002 and accepted in revised form 4 March 2003]

ABSTRACT

Temporal nanostructural fluctuations brought about by transient metastable atom-cluster formation during radiation-induced amorphizing transformation in the intermetallic compound NiTi, observed using a combination of high-resolution high-voltage electron microscopy and molecular dynamics simulation, were characterized in terms of power-law responses of non-equilibrium energy-dissipative systems. Within the framework of the multi-Lorentzian picture, the resultant power law also describes the multirelaxation time (i.e. cluster lifetime) distribution. In addition, a unified relation for the autocorrelation functions for such fluctuation phenomena is discussed.

§1. INTRODUCTION

Power-law responses of extended dynamic systems with both temporal and spatial degrees of freedom are well recognized in nature (Kadanoff 1966, Mandelbrot 1982, Bak *et al.* 1987, 1988, Kramer and Lobkovsky 1996, Sethna *et al.* 2001). Such systems commonly exist in chemistry, physics, biology and even in social sciences such as economics. The spatiotemporal power-law effects include crackling noise (for example Sethna *et al.* (2001)), for example $1/f$ noise or flicker noise in self-organized critical systems (Bak *et al.* 1987, 1988) and self-similarity or fractal property (Mandelbrot 1982), both occurring in a scale-invariant manner. A good understanding of the origin and stability of the spatiotemporal fluctuations would thus facilitate the physical interpretation of various phenomena, including noise-to-ordering transition (Shibrot and Muzzio 2001) and spatiotemporal patterning (Cross and Hohenberg 1993, Walgraef 1997) in energy-dissipative systems.

[†] Email: watanabe@loam-ms.eng.hokudai.ac.jp.

[‡] Present address: Fuji Electric Co. Ltd, 7, Yawata Kaigandori, Chiba 290-8511, Japan.

Recently, using a combination of *in-situ* observations inside a high-resolution high-voltage electron microscope and molecular dynamics (MD) simulation, the present authors studied the dynamics of electron irradiation-induced amorphizing transformation in the NiTi intermetallic compound (Watanabe *et al.* 2001, Koike *et al.* 2002). Metastable atomic clusters were found to form and disappear repeatedly in the irradiated structure, giving rise to nanoscale spatiotemporal fluctuations (Watanabe *et al.* 2001). It was suggested that these fluctuations represent non-equilibrium processes that occur during the amorphizing transformation, and that a high-energy particle irradiation field produced in a high-resolution high-voltage electron microscope provides a useful environment in which dynamic structural fluctuations can be investigated on an atomic scale.

In the present work, fast Fourier transform (FFT) power-spectrum analyses of structural fluctuations were performed in order to characterize their temporal responses. We are primarily concerned with the fluctuation spectra related to the system response rather than with the nature of individual metastable clusters. It is shown that such responses display a power-law behaviour, and a universal auto-correlation function can be formulated, which is obeyed by our various structural data. The present results provide a new insight into the multirelaxation dynamics of alloy systems under irradiation.

§2. EXPERIMENTAL AND MOLECULAR DYNAMICS SIMULATION PROCEDURES

Amorphous metallic alloys have traditionally been produced by rapid quenching from the liquid state, by vapour deposition and by electrodeposition techniques. More recently, the amorphous state has been found to be produced directly from the crystalline state by a variety of externally driven processes (Okamoto *et al.* 1999). Amorphization of intermetallic compounds by high-energy particle irradiation has been investigated extensively (Mori *et al.* 1984, Lam *et al.* 1997, Okamoto *et al.* 1999). Most of these investigations have utilized electron, X-ray or neutron scattering techniques to obtain information about the changes in the atomic structure that occur during the crystal-to-amorphous transition. A major limitation of the diffraction technique is that it provides only spatial and temporal averaged information, so that much of the information on the local fluctuations in the atomic structure is lost. However, the development of high-resolution high-voltage electron microscopes has made it possible to carry out *in-situ* real-time studies of radiation-induced structural changes on the atomic scale.

2.1. High-voltage electron microscopy experiment

NiTi samples used in the present study were supplied by the Furukawa Electric Co. Ltd, Tokyo, and were prepared from mechanically polished thin sheets (0.3 mm) having a Ni concentration of 51 at.%. Pre-annealing was carried out at 1173 K in a vacuum, followed by electropolishing of the central area of the disc of 3 mm diameter with a solution of 7% perchloric acid and 93% acetic acid. The annealing treatment produced polycrystalline NiTi (B2 structure) having a typical grain size of 10 μm . The transmission electron microscopy samples were irradiated with 1.25 MeV electrons (dose rate, 1.0×10^{24} electrons $\text{m}^{-2} \text{s}^{-1}$) at temperatures from 173 to 523 K in a recently installed high-voltage electron microscope (JEM-ARM1300) at Hokkaido University. The point-to-point resolution of this microscope is 0.12 nm. The flux profile of electron beam has a central maximum intensity region of approximately 0.2 μm in diameter, in which the dose rate can be considered to be constant.

During electron irradiation, high-resolution digital images taken near Scherzer defocus (for example William and Carter (1996, p. 465)) were video-recorded with a charge-coupled device camera. The minimum interval time for acquiring the images was $\frac{1}{30}$ s. FFT image analysis was used to investigate the amorphization process and to obtain local atomic ordering information. The FFT image might involve artefacts, particularly when the high-resolution electron microscopy (HREM) image itself is taken at out-of-focus condition, deviating from the true (projected) potential condition.

2.2. Molecular dynamics simulation of electron irradiation

MD and statistical analysis of the atomic structure were performed using the interatomic potentials derived by Sabochick and Lam (1991) on the basis of the embedded-atom method (Daw and Baskes 1984). A cubic system containing 1000 Ni atoms and 1000 Ti atoms, subjected to periodic boundary and constant-pressure conditions, was used. The atoms were arranged in a B2 lattice with the lattice parameter $a=0.2998$ nm. One Frenkel pair (FP) was created randomly in the crystal every $10 \Delta t$ (Δt is a MD time step, corresponding to 2×10^{-3} ps) for up to $2 \times 10^4 \Delta t$. The total number of FP insertions thus corresponds to a dose of 1.0 displacement per atom (dpa). Prior to statistical analyses, the system was equilibrated for $1 \times 10^4 \Delta t$ in order to relax the system, and several physical properties, including the system's volume, and potential and kinetic energies, were then evaluated during an additional $1 \times 10^4 \Delta t$. For comparison, we also used the same procedure for simulating the annealing effect (without FP insertion).

2.3. Analysis of molecular dynamics simulation results

Diffraction patterns and HREM images of the MD-generated atomic configurations were independently calculated using the multislice method (Ishizuka and Uyeda 1977), with the aid of Mac Tempas software (total resolution: <http://www.totalresolution.com>). Typical parameters for our high-voltage electron microscopy experiment, such as foil normal, sample thickness, accelerating voltage, spherical aberration coefficient C_s and defocus values, were used as input parameters. By through-focus and thickness simulation, we determined the sample thickness near one Scherzer defocus value (-57 nm) for our high-voltage electron microscope in order to assure the true projection condition, so that the Fourier transformed image of the calculated HREM image corresponds to the predicted diffraction pattern. For example, for the case in which the viewing direction is the foil normal direction $\langle 111 \rangle$, we used a sample thickness of 15 nm, an accelerating voltage of 1250 kV, $C_s=2.65$ mm, and a defocus value of (under focus) -57 nm. The Debye-Waller factors were set to equal weight (dw-fact parameter in MacTempas, 0.5) in the present calculation.

The power spectra of various temporal fluctuation data were calculated via FFT:

$$S(f) = \lim_{T \rightarrow \infty} \left(\left| \frac{1}{T} \int_0^T X(t) \exp(-ift) dt \right|^2 \right), \quad (1)$$

where f is the frequency and $X(t)$ is the fluctuation observable. These spectra were then averaged over different realizations. The present FFT study did not use pass filters, except for an appropriate rectangular window function, and the upper limit (maximum data time) and the lower limit (minimum time increment) of T in equation (1) were set depending on the obtained data.

§3. RADIATION-INDUCED AMORPHIZATION

3.1. Structural fluctuation: local amorphization parameter and changes in volume and potential energy

In the present study of structural fluctuations, we introduced a *local amorphization parameter* (LAP) $P(t)$ (Watanabe *et al.* 2001), to measure the extent of amorphization at time t , via the equations

$$P(t) = \frac{I(t) - I(0)}{1 - I(0)} \quad (2)$$

and

$$I(t) = \frac{I_{\text{rest}}(t)}{I_{\text{F}}(t)}, \quad (3)$$

where $I_{\text{F}}(t)$ is the integrated intensity at fundamental spots in the FFT pattern and $I_{\text{rest}}(t)$ is the (total) intensity normalized by the area of the diffuse-halo region that does not contain any fundamental spots (figure 1 (b)). Like $I(t)$, $P(t)$ varies from 0 to 1 as the sample passes from the crystalline state ($P=0$; assured at $t=0$) to the completely amorphous state ($P=1$). The subtracting constant term $I(0)$ in equation (2) for $P(t)$ reflects ‘the background noise’, which could ideally be neglected. However, in the actual experiment, there exists a background noise arising from unwanted agitations and, possibly, an artefact in FFT when dealing with finite-sized regional data.

Figure 1 (a) illustrates an example for the dose-dependent fluctuations at 300 K of the local amorphization parameter P and typical high-resolution HVEM images taken during electron irradiation, with the corresponding FFT patterns given in the inset images. The foil orientation was $\langle 111 \rangle$, which was also the electron incidence direction. The intensities of the spots and the diffuse halo were integrated over a 10 pixel width in 256×256 images (12 nm \times 12 nm in real space). In the amorphization process, nanometre-sized atom clusters of different sizes and shapes were observed to form stochastically and to annihilate in the images. Correspondingly, extra spots appeared and disappeared in the FFT patterns (e.g. as indicated by arrows near the diffuse halo in figure 1 (a)B).

In a previous report (Watanabe *et al.* 2001), in place of I in equation (3), we used

$$I'(t) = \frac{I_{\text{H}}(t)}{I_{\text{F}}(t)}, \quad (4)$$

where $I_{\text{H}}(t)$ is the integrated intensity at an arbitrary point H on the diffuse halo and $I_{\text{F}}(t)$ is the integrated intensity at the position of the $\{110\}$ fundamental spot in the FFT pattern. It follows that $I_{\text{H}}(t) = I_{\text{F}}(t)$ when the sample is completely amorphous and $I_{\text{H}}(t) = 0$ for the completely crystalline state. We used $I(t)$ instead of the original $I'(t)$ in the present study because, unlike the latter which only samples some chosen k -space points, the former reflects the average information for the entire spatial region of an HREM image. In fact, $I'(t)$ should merge to $I(t)$ when all orientations are considered along the halo. To provide a comparison, we checked the reliability of our P values by substituting I' for I in equation (2). Although the deviation is occasionally large, the P values for diametrically opposite pairs were almost always identical, the reason being that, in a FFT diffractogram, the intensities of the oppos-

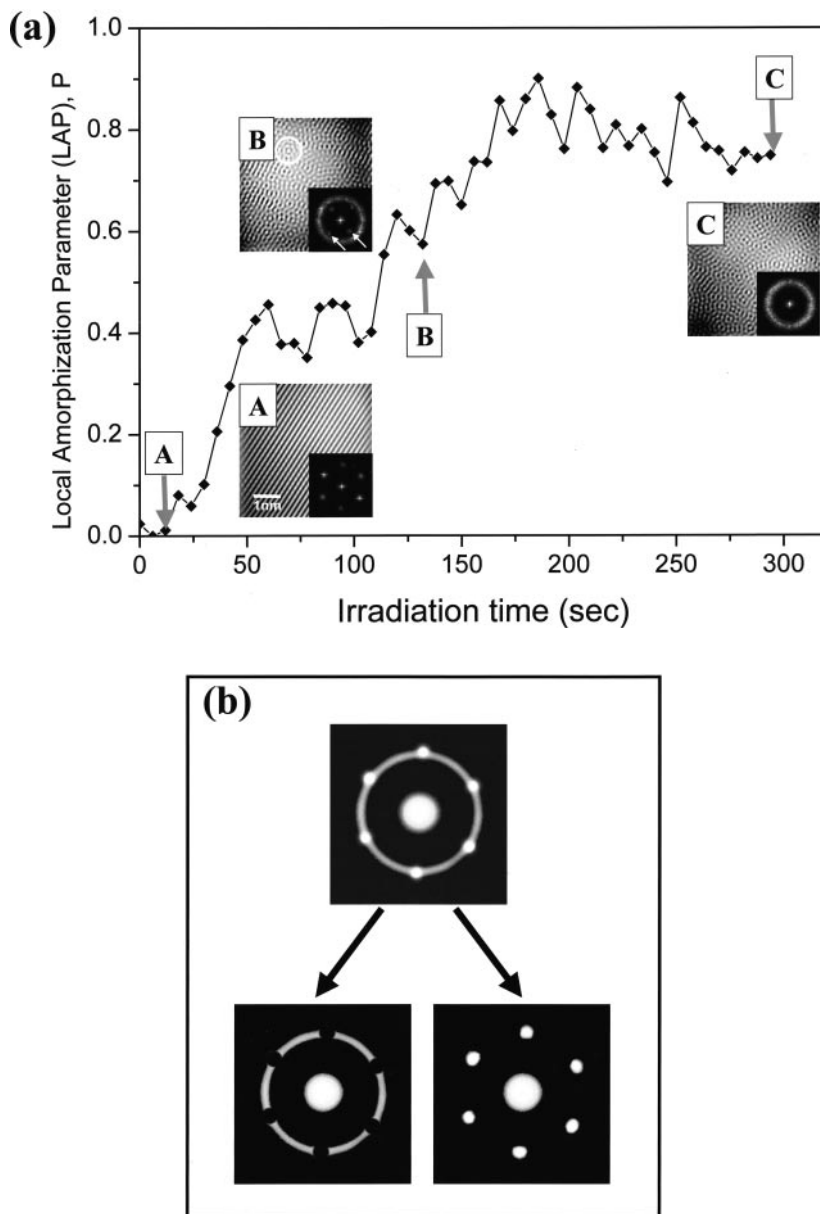


Figure 1. (a) Experimentally observed structural fluctuations during radiation-induced amorphizing transformation in NiTi at 300 K: dose-dependent fluctuations in the local LAP, P , and high-resolution images (insets A–C) obtained at three different doses, together with the corresponding FFT diffractograms. The foil normal is (111). (b) Data sampling method in the reciprocal space used to obtain a value for P .

ing spots must be equal according to the Friedel law. The allowance of the measurement on the averaged P was approximately ± 0.1 . Still, fluctuation was evident. In order to perform more accurate dynamic measurements of P , recent sophisticated techniques such as phase electron microscopy by defocus-image modulation (Takai *et al.* 2001) may be necessary.

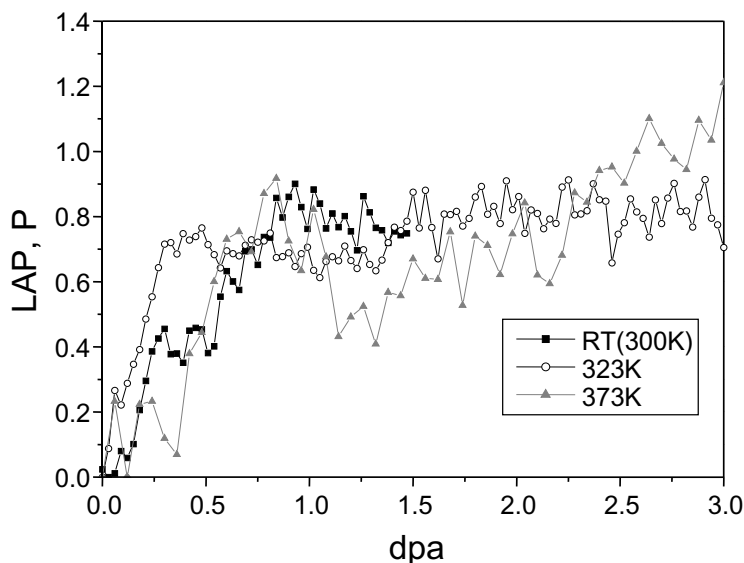


Figure 2. Fluctuations in P during radiation-induced amorphizing transformation of NiTi under HVEM electron irradiation at 300, 323 and 373 K: RT, room temperature. Here, 1 dpa corresponds to irradiation for 200 s.

The LAP values P fluctuate around a steady-state value after some dose. The onset dose for the steady state, near 0.9 dpa, in figure 1 corresponds macroscopically to the amorphous state (but not atomistically because of the existence of nanoscale clusters). The fluctuations in LAP at different temperatures were similar in both the HVEM experiment (figure 2) and the MD simulation (figure 3). From the MD-generated configurations, the values of P were also evaluated using equation (2) via the same method as in the analysis of the experimental data. We used the diffraction pattern rather than a FFT diffractogram for the MD simulation because diffraction is not sensitive to the defocus value (it only depends on thickness), and because the FFT diffractogram becomes noisy with artefacts due to the relatively small number of atoms in MD simulation.

The values of P in the figures exceed 1.0 (for complete amorphization) from time to time because the intensities of the initially chosen fundamental spots became weaker than those formed in other portions of the diffuse halo. Although the value for P in the amorphous state seems to be ill defined because the fundamental spot becomes indistinguishable, the fluctuation in P in the amorphous state still occurs owing to random nanocluster formation, by which the recovery of the fundamental spots is generated stochastically. For clarity concerning the characteristics of fluctuation, we shall later carry out a power spectrum analysis on the fluctuation, dividing the data range into before- and after-amorphization portions. Moreover, in order to ascertain such structural fluctuation and to evaluate the critical dose for amorphization, we further investigated the changes in the potential and volume of the system via MD simulation. Figures 4 and 5 show MD simulation results for potential and volume respectively of the system with respect to dose. The critical dose for amorphization, determined from the amorphization parameter, volume and potential, is approximately 0.25 dpa.

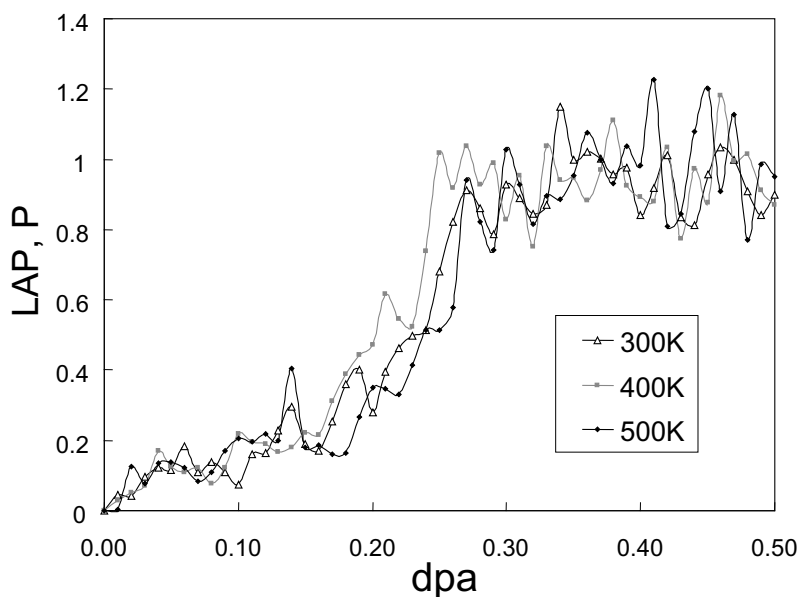


Figure 3. Dose-dependent fluctuations in P , observed in MD simulation at 300, 400 and 500 K. Parameters for image simulation are as follows: foil normal, $\langle 111 \rangle$; sample thickness, 15 nm; accelerating voltage, 1250 kV; $C_s = 2.65$ mm; defocus, -57 nm.

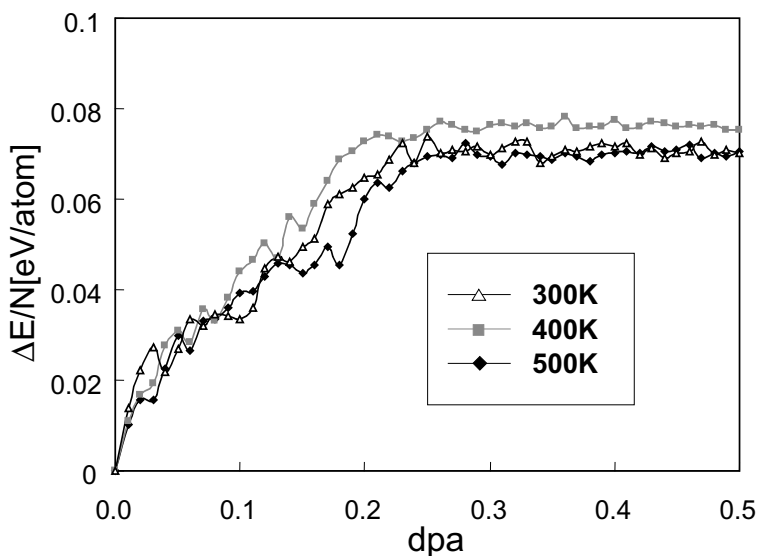


Figure 4. Simulated temporal fluctuations in the total potential energy (per atom), $\Delta E/N$ at 300, 400 and 500 K.

In general, the experimentally observed fluctuations (see figure 2) showed longer wavelengths and higher critical doses at higher temperatures because these factors are influenced not only by spontaneous defect recombination but also by radiation-induced diffusional processes which are very difficult to observe in MD. The period of these fluctuations increases with increasing temperature and therefore

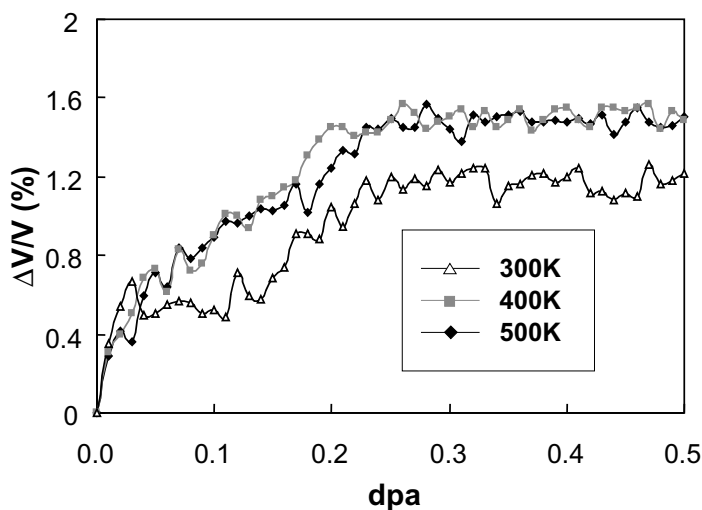


Figure 5. Simulated temporal fluctuations in the volume change, $\Delta V/V$ at 300, 400 and 500 K.

may be a measure of the mean lifetime of nanometre-sized crystalline regions that appear and disappear during irradiation. The increased period of fluctuations with increasing temperature is consistent with the fact that higher temperatures favour the recovery of the crystalline state over the formation of the amorphous phase. Indeed, above 400 K, the temperature region in which thermal recovery processes dominate over athermal disordering events, NiTi was not completely amorphized by HVEM irradiation and only chemical disordering was observed.

3.2. Chemical and topological disordering

In order to investigate chemical disordering, we monitored the disappearance of $\{100\}$ long-range-order spots in the diffraction patterns as viewed from the $\langle 110 \rangle$ direction, which is shown as MD results in figure 6. Calculated images and diffraction patterns are shown together in series as a function of dose level. Because of the extinction rule for the B2 structure (space group, $Pm3m$), the $\{hkl\}$ diffraction spot vanishes for complete chemical disorder when $h+k+l$ is odd but does not vanish in the chemically ordered state, owing to the $f_{\text{Ni}} - f_{\text{Ti}}$ contribution, where the f s are the atomic scattering factors. Spots for which $h+k+l$ is even do not vanish with chemical disordering and contribute as fundamental spots. Therefore, the $\{001\}$ spots in figure 6 become weak at first by chemical disordering and then diminish completely near 0.15 dpa. Subsequently, the fundamental spots such as $\{112\}$, $\{002\}$ and $\{110\}$ vanish owing to the topological disordering stage prior to amorphization. It is interesting that, during chemical disordering, diffuse scattering, which is an indication of short-range ordering (for example Banerjee *et al.* 1984, 1989), was observed (see for example the diamond-shaped spots along the lines between $\{110\}$ and $\{002\}$ in figure 6, and spots outlined by white circles). This is probably the signature of an inherent atomic clustering (or bonding) in the process of amorphization, which will be discussed in the next section.

The response of the intermetallic compound NiTi to irradiation in the present experimental and simulation studies can be summarized as follows. Chemical

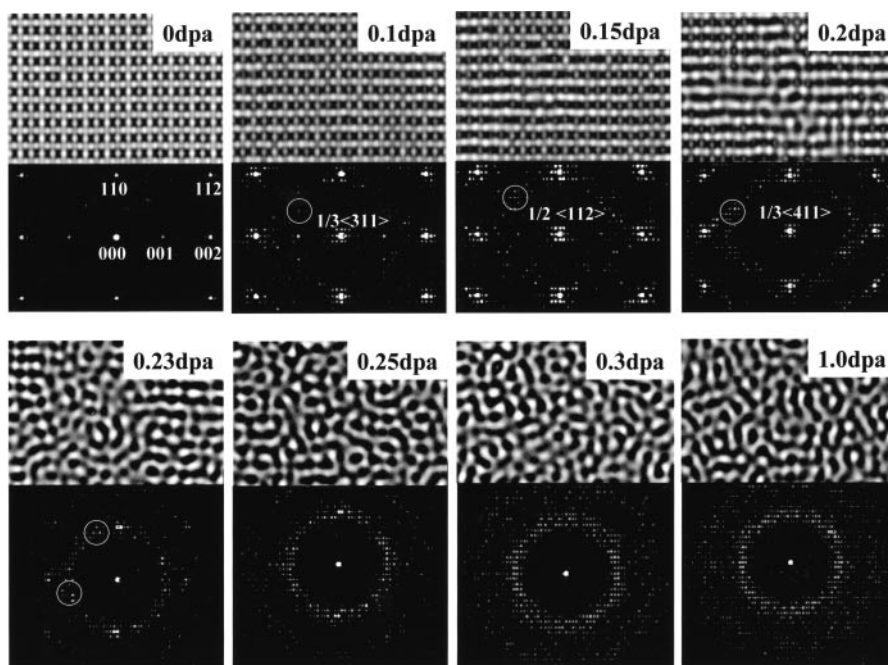


Figure 6. Calculated dynamic changes in the atomic structural images and corresponding diffraction patterns by MD simulation at 300 K to 1 dpa. The same parameters as in figure 3 are used.

disordering occurs first, and then topological disordering begins and proceeds until amorphization is complete. The corresponding ranges of irradiation doses in MD simulation are 0–0.15 dpa for chemical disordering and 0.15–0.25 dpa for topological disordering, leading to amorphization. The critical dose for amorphization is thus approximately 0.25 dpa. Experimentally (see figure 1), the observed stages were vague but appeared to occur over wider ranges of dpa: firstly, the chemical disordering stage (0–0.4 dpa), and then the topological disordering stage (0.4–0.9 dpa). Both experimental and MD results show that the fluctuations increase in amplitude in the second topological disordering stage and continue to occur even after the system has become completely amorphous. The requirement of FP creation for amorphization to occur in the NiTi compound was discussed in a previous MD simulation (Sabochnik and Lam 1991) and is reconfirmed in the present study because chemical disordering alone cannot bring about the topological disorder.

3.3. Atomic configuration of the clusters: radial distribution function and inherent bonding

Changes in the inherent structure (for glassy systems, see for example Stillinger (1995) and Angell *et al.* (2000)) of atom clusters during a radiation-induced crystalline-to-amorphous transition are illustrated for MD results in figure 7. As shown by the total radial distribution function $g(r)$ in figure 7(a), long-range ordering diminishes with increasing chemical disorder, and inherent medium-range ordering develops when amorphization occurs. In fact, in figure 7(a), the second peak near 0.46 nm on the 0.5 dpa curve, in the shaded region, shifts to longer distances, compared with that on the 0.15 dpa curve. The original position before irradiation was at

0.42 nm, corresponding to twice the $\{110\}$ interplane distance. The critical dose for amorphization is again evaluated to be approximately 0.25 dpa. No significant changes are recognized in $g(r)$ thereafter, and the distribution is identical with that obtained after quenching from a liquid state to 160 K. Figures 7(b)–(d) show pair distribution functions for Ni–Ni, Ni–Ti and Ti–Ti atoms respectively at various dose levels. To extract and monitor the inherent bondings, we traced the peak development near 0.46 nm for Ti–Ti atomic bonds with dose increment. Snapshots of the atomic coordinates and bonding arrangements responsible for such intermediate ordering are shown for Ti–Ti interatomic bonds between 0.465 and 0.470 nm

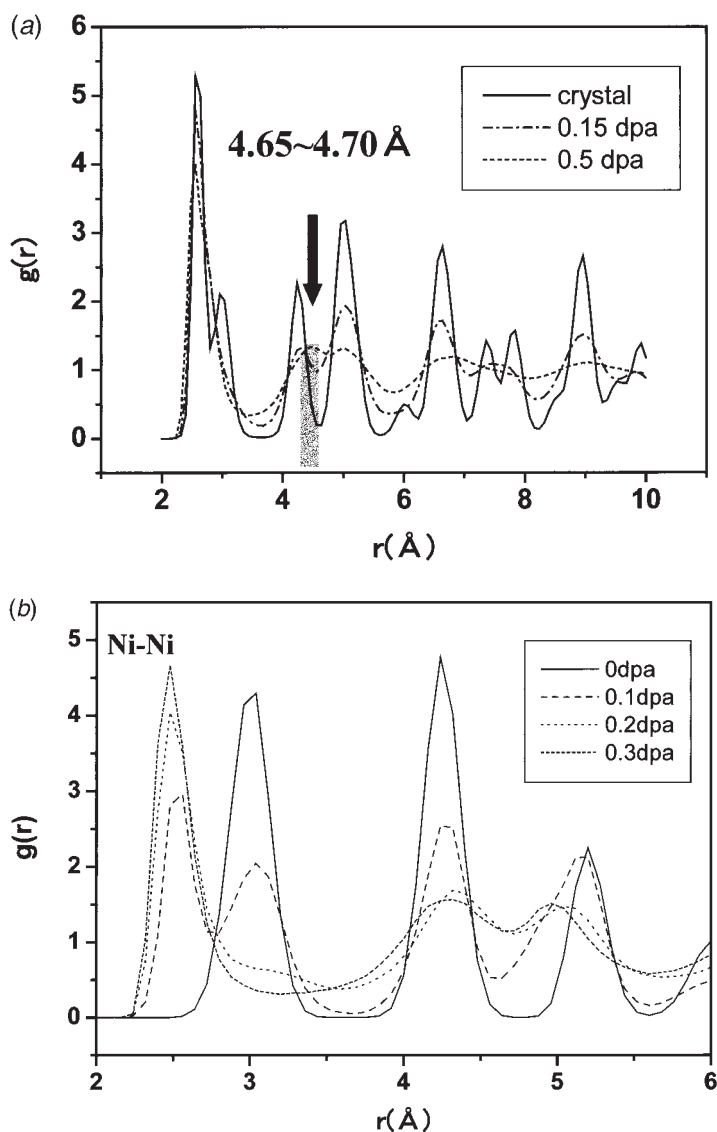


Figure 7. Simulated radial distribution functions $g(r)$ at three doses 0, 0.15 and 0.5 dpa: (a) total $g(r)$; (b) partial $g(r)$ for Ni–Ni pairs; (c) partial $g(r)$ for Ni–Ti pairs; (d) partial $g(r)$ for Ti–Ti pairs.

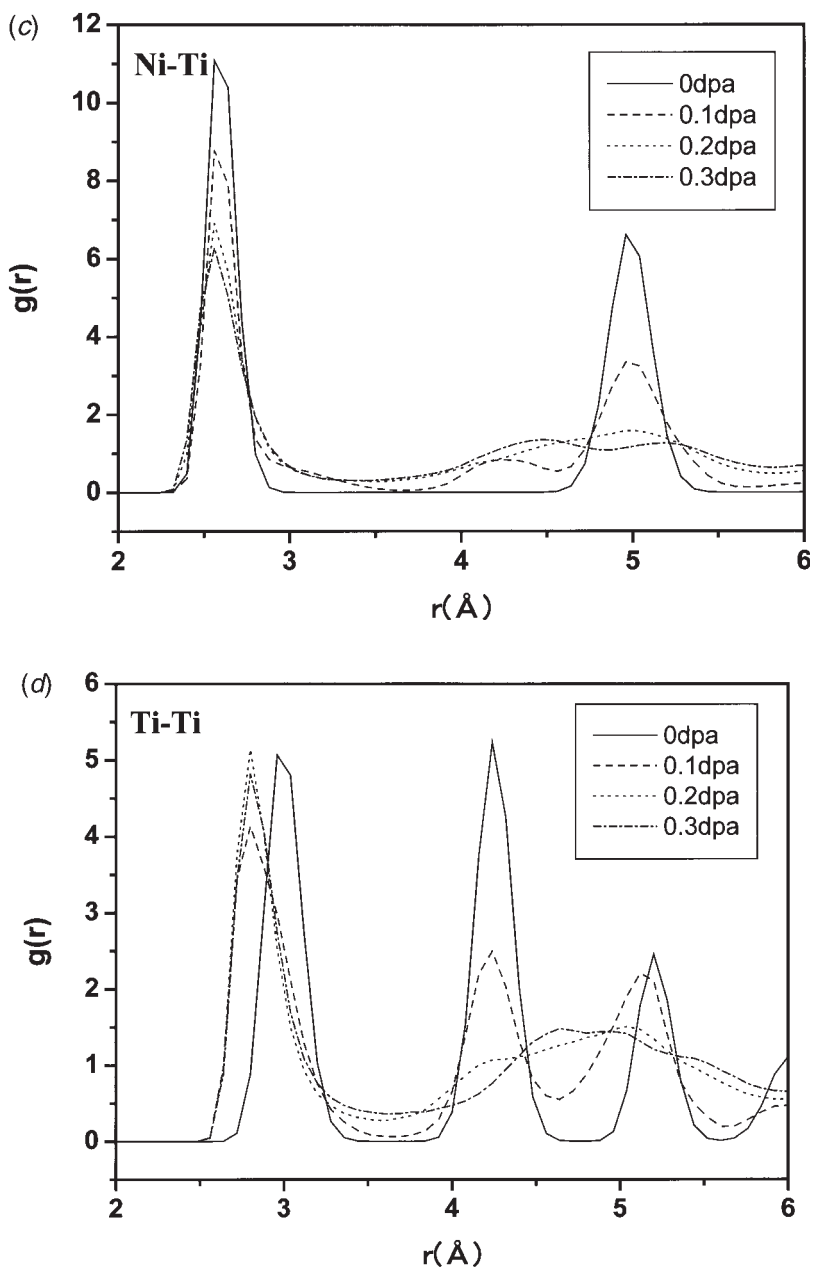


Figure 7. (continued)

in figure 8. The corresponding bond number increase is shown in figure 9. Not only does the bond number increase with increasing damage dose (figure 9), but also the bonding arrangement itself (e.g. figure 8) changes at every moment, which is believed to lead to nanostructural fluctuations. The fluctuation continues even after the completion of amorphization at 0.25 dpa.

Although we have not extracted individual cluster structures and their corresponding size distribution, the present results, which appear to be in accord with

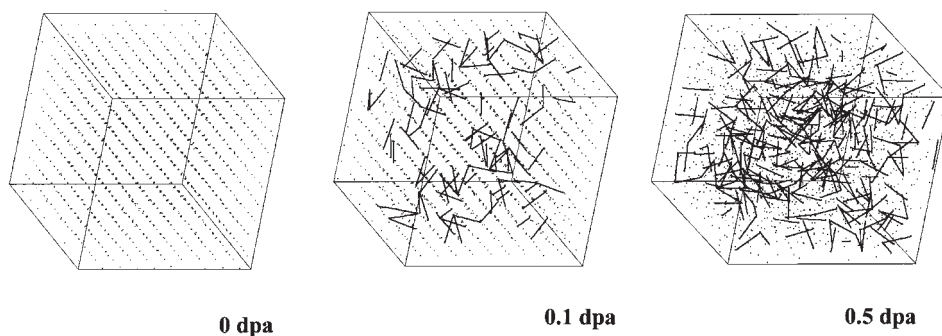


Figure 8. Snapshots of the three-dimensional configuration of Ti–Ti interatomic bonds of length between 0.465 and 0.470 nm.

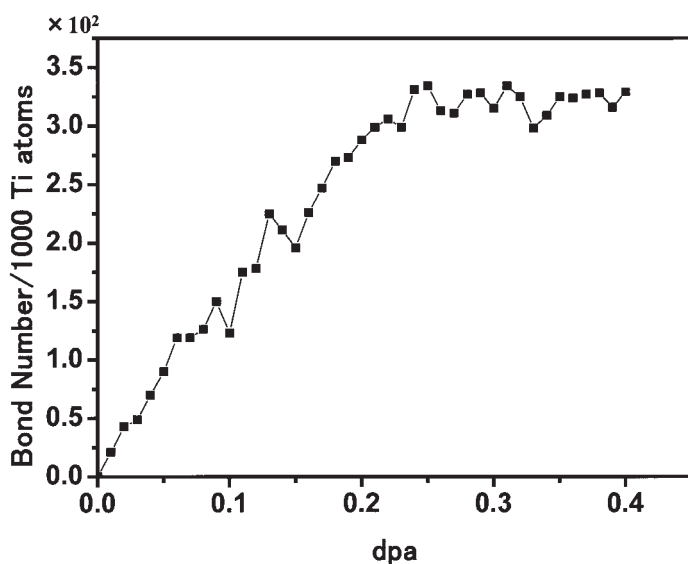


Figure 9. Dose dependence and fluctuation in the Ti–Ti bond number during irradiation. The corresponding inherent bond number tends to increase as the amorphization proceeds and tends to saturate after the critical dose (0.25 dpa).

the landscape model (Stillinger 1995, Debenedetti and Stillinger 2001), indicate transitions between the basins of inherent metastable states in a glass-forming system. In other words, the stochastic formation and annihilation of the inherent nanocrystalline clusters are responsible for these fluctuations, which are probably related to transitions between the ideal-glass state (Kauzmann 1948) and metastable unrelaxed states in an energy-dissipative system under irradiation. Such nanocrystalline clusters in a transition state can have intrinsic short-range-order atomic arrangements, which give rise to the extra spots observed at low doses in the FFT pattern (e.g. as indicated by arrows in figure 1).

§4. TEMPORAL FLUCTUATION AND ITS ANALYSIS

In this section, we analyse the fluctuation data by their power spectra and auto-correlation function. We do not attempt to discuss the physical model describing

each stochastic event; rather, we propose a power law that would facilitate the search for a physical model.

4.1. Power-spectrum analysis

Shown in figure 10 is a temporal power-law behaviour of the fluctuations, $S \propto f^m$, obtained from the FFT power spectra S of the experimental LAP data in figure 2 at 300, 323 and 373 K. Because the amorphization occurred so quickly at low temperatures (irradiation for 30 s at 173 K, i.e. 0.15 dpa), we were unable to obtain a sufficient number of data points. The quantity f in the abscissa of the log–log plot is defined as 1/dpa and corresponds linearly to hertz (1/second) because the irradiation was performed under a constant dose rate, 1 dpa corresponding to roughly 200 s. Using the method of least squares, for example in the case of 300 K, the slope of the straight line yields $m = -1.87 \pm 0.19$ (errors are one standard deviation) as the power, that is an $f^{-1.87}$ spectrum is obtained. Although the temperature dependence of the slope is not characterized, the data points shift to lower frequencies with increasing temperature; that is, the time interval increases.

In order to examine in further detail whether fluctuations under irradiation involve a multirelaxation dynamics and/or a mode-coupling behaviour (Stillinger 1995, Nayak *et al.* 1995, Angell *et al.* 2000, Debenedetti and Stillinger 2001), FFT power spectrum analyses of the local amorphization parameter P , and the potential energy and volume of the system were performed using the dose-dependent (time-wise) data obtained from the MD simulation in figures 3, 4 and 5 respectively.

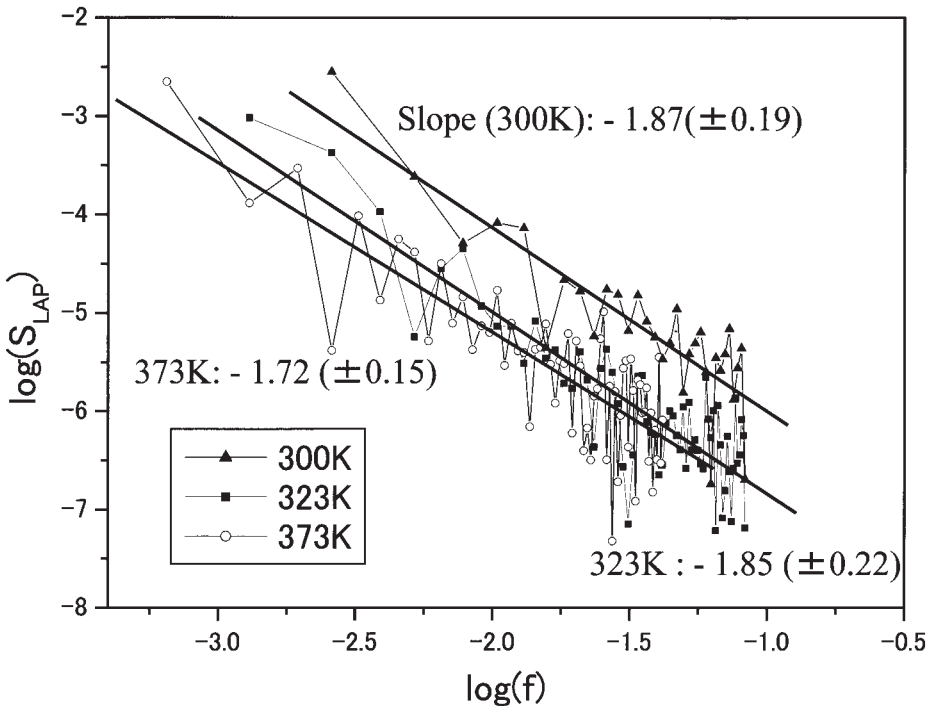


Figure 10. log–log plot of the FFT power spectrum of the fluctuations in P (S_{LAP}) experimentally measured at 300, 323 and 373 K, as shown in figure 2. The slope of the line is $m \approx -1.8$.

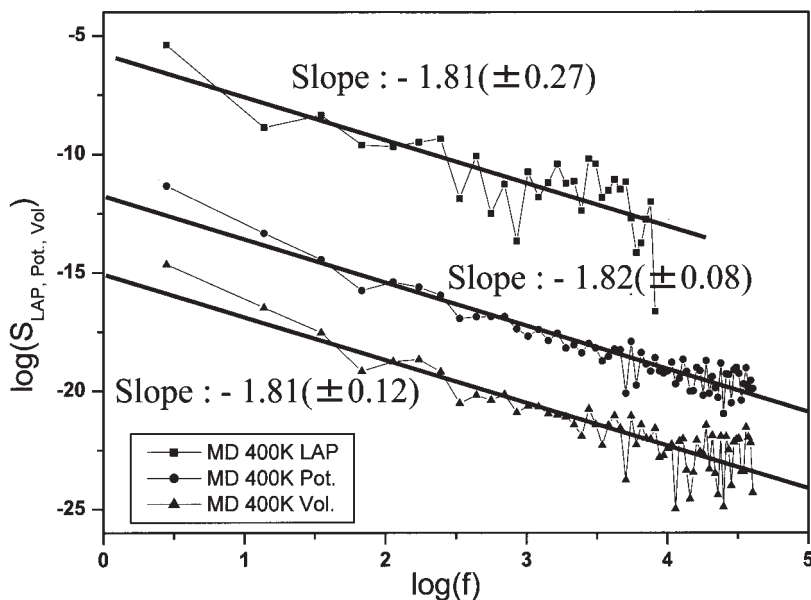


Figure 11. log-log plot of the MD-simulated power spectra S_{LAP} , S_{Vol} and S_{Pot} of fluctuations in the local amorphization parameter, volume and potential energy respectively, using the dose-dependent fluctuation data in figures 3–5. The power value $m \approx -1.8$ is common for all fluctuating quantities.

Figures 11 (a), (b) and (c) show the power spectra of local amorphization (S_{LAP}) total potential (S_{Pot}) and volume (S_{Vol}) respectively for irradiation at 400 K. The temporal power-law behaviour described by $m = -1.8$ was found to be common for all three physical properties: -1.82 ± 0.08 for potential-energy fluctuations, -1.81 ± 0.27 for fluctuations in P , and -1.81 ± 0.12 for volume change, which is consistent with the experimental finding, $m = -1.87 \pm 0.19$ (see figure 10). Moreover, the power value obtained from the inherent bonding fluctuation in figure 9 was $m = -1.76 \pm 0.13$. An extended evaluation of the potential energy data up to 1.0 dpa (figure 12 (a)) yielded $m = -1.85 \pm 0.06$, with a straight line in the log-log plot over more than two orders of magnitude in the frequency range. Within evaluation errors, the power m appears to be temperature independent over the temperature range under investigation; for example, the analysis of potential-energy fluctuations in figure 4 yielded $m = -1.91 \pm 0.15$ (at 300 K), -1.82 ± 0.08 (400 K), and -1.76 ± 0.24 (500 K).

In the above power spectral analysis, we used the entire fluctuation data range, whereas figure 12 shows the results of regional data, both during the disordering state and after amorphization. Figure 12 (a) shows the original fluctuation data for the potential energy in the two regions, bounded at the critical dose of 0.25 dpa. The power spectrum using the data of region I (0–0.25 dpa) is shown in figure 12 (b), and those for region II (0.25–1.0 dpa) are shown in figure 12 (c). The power values shown in figures 12 (b) and (c) are almost identical with those shown in figure 11 for the entire data region, indicating that the power-law signature induced by irradiation (FP insertion) is common throughout the amorphization process. Furthermore, we also investigated the annealing behaviours of both the crystalline and the amorphous states. The respective power values are $m = -0.10 \pm 0.11$ (figure 13 (a)) and $m = -1.81 \pm 0.13$ (figure 13 (b)), indicating that these fluctuations are characterized

by a white-noise-like behaviour for the crystalline state, and the behaviour found for the irradiation case also holds for the amorphous state. The latter result is surprising because this means that the thermally dissipated amorphous state and irradiation-induced amorphization behave in similar manners. We do believe that the inherent bonding in the amorphous state is usually responsible for such characteristic responses in both cases.

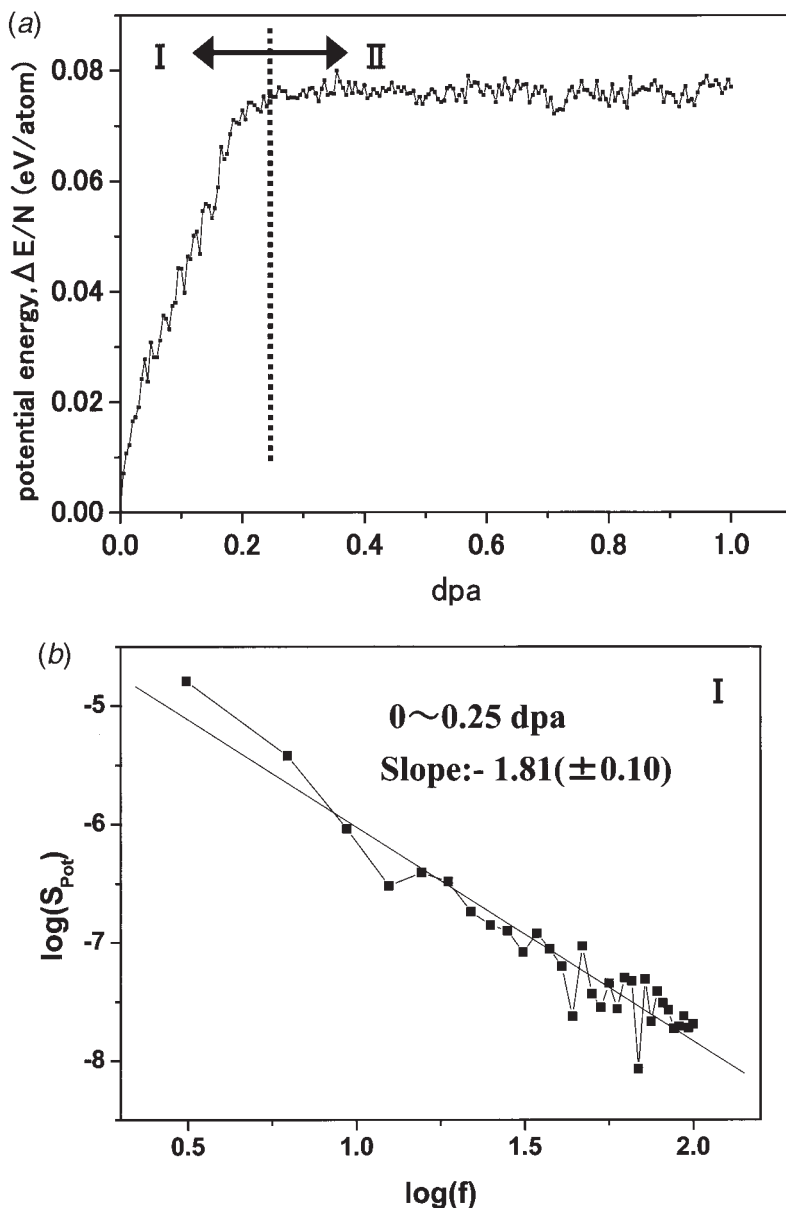
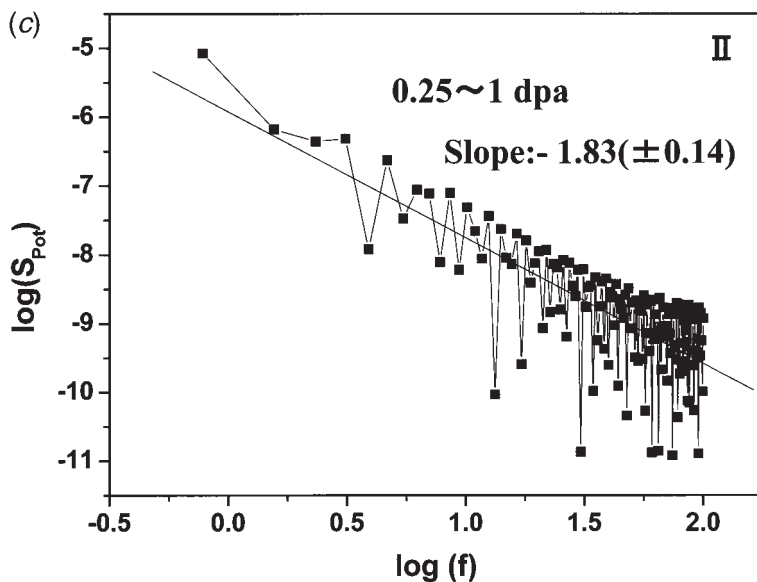


Figure 12. (a) MD results for potential energy versus dose at 400 K, plotted at every 0.01 dpa. (b) Power spectrum of fluctuations in region I, between 0 and 0.25 dpa. (c) Power spectrum of fluctuations in region II, between 0.25 and 1.0 dpa.

Figure 12. (*continued*)

The power values obtained in the present study, except for the annealing of the crystalline state, all fall within the range $-2 < m < -1$. The results in the power-law analysis of non-zero and deviation from -2 indicate that the fluctuation is neither white noise (a power value of zero is indicative of ‘equilibrium fluctuation’) nor a simple Lorentzian (power of -2) that has a decay constant. This indicates that the observed fluctuation is a non-equilibrium process with many-body effects (multirelaxation), leading to a distribution of relaxation times. Identifying the fluctuation types is crucial in the noise statistics, and the usual procedure used is the power-spectrum analysis or, more directly, the examination of the autocorrelation. For example, simple diffusion of an element in the crystalline state is known to have a power spectrum of -2 in the high-frequency region and a single Lorentzian form in its temporal autocorrelation. In the next section, we derive the power-law distribution of the relaxation times, based on the multi-Lorentzian picture, and analyse the autocorrelation function of the fluctuation data.

4.2. Theory of multi-Lorentzian noise and power law

The power-law response is suggestive of a scaling picture for the alloy system under study. For example, the MD-simulated fluctuations, which occur on a picosecond time scale, exhibit periods of approximately 0.04 dpa, whereas those observed experimentally at low temperatures occur on a second time scale, with periods of about 0.1 dpa. This indicates that both the computer-simulated and the experimentally observed fluctuations are intrinsically governed by equivalent short-time-scale events which involve local multiatom relaxations driven by spontaneous mutual recombination of interstitials and vacancies.

Determining the power spectra and the corresponding autocorrelation function form in $1/f$ fluctuation was initiated by van der Ziel (1950) in his flicker noise study in a semiconductor device. Hogge and Bobbert (1997) recently proposed an explicit

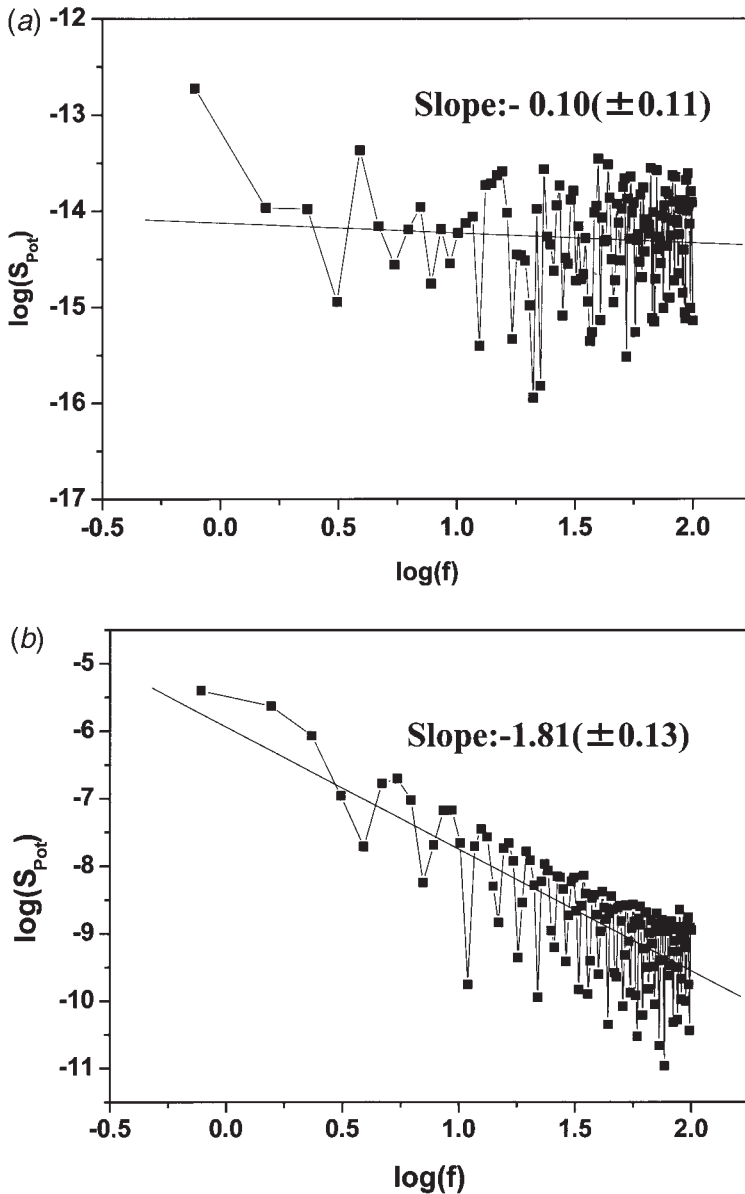


Figure 13. Power spectral analysis on potential-energy fluctuations during annealing of (a) the crystalline compound and (b) the amorphous compound.

function of time-logarithmic form based on multi-Lorentzian spectra, assuming a relaxation time distribution inversely proportional to itself, that is $1/\tau$. Although Hogge and Bobbert (1997) discussed the noise yielding exact $1/f$ frequency dependence, most cases of $1/f$ noise spectra deviate from this dependence; in fact, we often find the frequency power in the form $f^{-\beta}$, where $0 < \beta < 2$ (Dutta and Horn 1981, Bak *et al.* 1987, 1988). In their original work on self-organized criticality, Bak *et al.* (1987, 1988) discussed $f^{-\beta}$ noise and a power-law distribution of relaxation time (Bak *et al.* referred to this as a cluster lifetime distribution) of $\tau^{-\alpha}$ type, yielding

the scaling invariance in the power spectra in the form $f^{-2+\alpha}$, with $0 < \alpha < 1$, with m being defined as $m = -\beta = -2 + \alpha$. For example, the power $m = -1.8$ in the frequency should yield $\alpha = 0.2$ in order to describe the relaxation lifetime distribution $\tau^{-\alpha}$.

On the basis of the above-mentioned multirelaxation picture involving different cluster lifetimes, the distribution of which obeys the power law $\tau^{-\alpha}$, we obtained the relation for power spectra and the corresponding autocorrelation function (S. Watanabe 2003, unpublished). The derivation of the former hinges on the assumption that the relaxation time of the Lorentzian spectrum, presumably the cluster lifetimes, be distributed in a power form over a wide time range.

The power law for multi-Lorentzian spectra, having a relaxation time distribution of $\tau^{-\alpha}$, is expressed by

$$S(f) = Af^{-2+\alpha}, \tag{5}$$

with

$$A = \frac{(1 - \alpha)\overline{X^2}}{\tau_2^{1-\alpha} - \tau_1^{1-\alpha}} (2\pi)^{\alpha-1} \operatorname{cosec}\left(\frac{\alpha\pi}{2}\right).$$

Here, τ_1 and τ_2 are the lower and upper limits respectively of the relaxation time and $\overline{X^2}$ is the variance of the fluctuating quantity. Equation (5) is valid when

$$0 < \alpha < 2 \quad \text{and} \quad \alpha \neq 1. \tag{6}$$

The scaling relation in a temporal autocorrelation function $\psi(t)$ of such multi-Lorentzian spectra is expressed as

$$\frac{\psi(t)}{\psi(0)} = \begin{cases} 1 - \left(\frac{t}{\tau_0}\right)^{1-\alpha}, & t \leq \tau_0, \\ 0, & t > \tau_0, \end{cases} \tag{7}$$

where $0 < \alpha < 1$, and τ_0 is defined as the loss-of-memory time, given by

$$\psi(\tau_0) = 0. \tag{8}$$

The explicit form of the τ_0 parameter is derived as a function of α using a Γ function:

$$\tau_0 = \left(\frac{\tau_2^{1-\alpha} - \tau_1^{1-\alpha}}{\Gamma(\alpha)}\right)^{1/(1-\alpha)}. \tag{9}$$

Equations (5)–(9) are obtained by directly evaluating the power spectra and the temporal autocorrelation function of a multi-Lorentzian noise defined as

$$S(f) = \overline{X^2} \int_{\tau_1}^{\tau_2} g(\tau) \frac{4\tau}{1 + (2\pi f\tau)^2} d\tau \tag{10}$$

and

$$\psi(t) = \overline{X^2} \int_{\tau_1}^{\tau_2} g(\tau) \exp\left(-\frac{t}{\tau}\right) d\tau \tag{11}$$

respectively. Here, a weight function of the lifetime distribution in the power form is introduced:

$$g(\tau) = a\tau^{-\alpha}, \tag{12}$$

where a must satisfy the normalization condition

$$1 = \int_{\tau_1}^{\tau_2} g(\tau) d\tau = \int_{\tau_1}^{\tau_2} a\tau^{-\alpha} d\tau = \frac{a}{1-\alpha} (\tau_2^{1-\alpha} - \tau_1^{1-\alpha}). \tag{13}$$

We can show that the Fourier transform (with an appropriate frequency cut-off) of the autocorrelation functions given by equation (7) yields the correct power spectrum $f^{-2+\alpha}$ form of equation (5). Using the Wiener–Khinchine law (for example Hogge and Bobbert 1997) in the derivative form

$$\begin{aligned} S_\tau(f) &= 4 \int_0^\infty \psi_\tau(t) \cos(2\pi ft) dt \\ &= -\frac{4}{(2\pi f)^2} \int_0^\infty \psi'_\tau(x) \sin x dx \quad (x \equiv 2\pi ft), \end{aligned} \tag{14}$$

the corresponding power spectrum for $0 < \alpha < 1$ with a higher-frequency cut-off is calculated as

$$\begin{aligned} S(f) &= -\frac{4}{(2\pi f)^2} \int_0^{2\pi f} \psi'(x) \sin x dx \\ &= \frac{4a\bar{X}^2 \Gamma(\alpha)}{(2\pi f)^{2-\alpha}} \left(\frac{\pi}{2\Gamma(\alpha) \sin(\alpha\pi/2)} - \int_{2\pi f}^\infty x^{-\alpha} \sin x dx \right). \end{aligned} \tag{15}$$

In the high-frequency limit ($2\pi f \gg 1$), the second term can be neglected because the integrand ($\sin(x)/x^\alpha$) becomes small for $x \geq 2\pi f \gg 1$, and one obtains

$$S(f) \approx \frac{a\bar{X}^2}{(2\pi)^{1-\alpha} \sin(\alpha\pi/2)} f^{-2+\alpha} \equiv A f^{-2+\alpha}, \tag{16}$$

which is the same as equation (5). In the next section, we analyse our fluctuation data on the basis of this relation.

4.3. Autocorrelation function and scaling relation

The scaling plots of the autocorrelation functions (equation (7)) for fluctuating data with, for example $\alpha = 0.2$, that is an $f^{-1.8}$ power law, are compared with those for the experimental fluctuation data and the MD simulation results in figure 14. The logarithmic plot of $\psi(t)/\psi(0)$ is a simple straight line for a ‘single Lorentzian noise’ and its autocorrelation function does not yield a finite loss-of-memory time. For a multi-Lorentzian, however, the plot deviates from straight line and shows a ‘decay’ near the loss-of-memory time ($t/\tau_0 = 1$). All the autocorrelation data were obtained by Fourier transformation of the power spectra, and those in the central envelope region (real and positive) are plotted. Good agreement with the predicted lines (equation (7)) is also observed for fluctuation data with other values of α . The values of τ_0 were derived from an extrapolation of the experimental and simulation data to yield $\psi(\tau_0) = 0$.

The τ_0 values, the characteristic time constants, obtained for the experimental data and MD simulation results are approximately 1.5 dpa (about 300 s) and 0.5 dpa (about 200 ps) respectively. The temporal scaling plots of the autocorrelation function are in good agreement with each other, depending only on the choice of α values, which are determined beforehand from the slopes of the power-spectral log–log plots. Although we have not directly measured the cluster lifetime distribution of

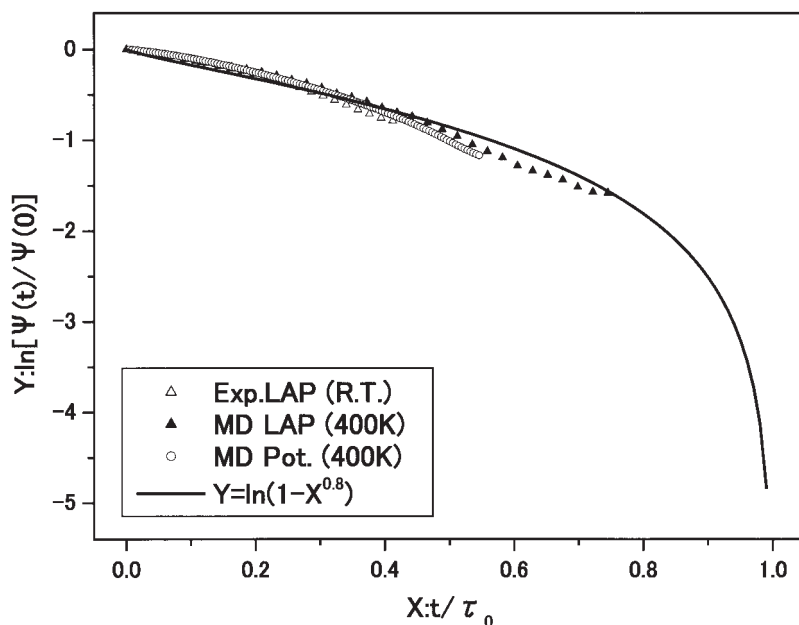


Figure 14. Scaling plot (with natural logarithmic form) of the autocorrelation function, $\psi(t)/\psi(0) = 1 - (t/\tau_0)^{1-\alpha}$, for the fluctuating quantities, with $\alpha=0.2$: R.T., room temperature.

the form $\tau^{-\alpha}$, the present results imply a multirelaxation dynamics, based on our multi-Lorentzian picture and the observed universal scaling behaviour of the structural fluctuations.

§5. CONCLUSION AND REMARKS

Dynamic observations of the radiation-induced amorphization process in NiTi were carried out via high-resolution HVEM and MD simulations. Nanometre-sized clusters were found to appear and disappear in the irradiated region. Temporal fluctuations during irradiation were manifested through the dose-dependent local amorphization parameter in the calculated potential energy, volume and inherent cluster bonding. The random formation and annihilation of such inherent nanoclusters are believed to be responsible for these fluctuations, which appear to be related to transitions between the ideal glass state and metastable unrelaxed states in an energy-dissipative system under irradiation.

The observed fluctuations ($\alpha=0.1-0.3$) obey a universal power law: $S(f) = Af^{-2+\alpha}$ for power spectra and $\psi(t)/\psi(0) = 1 - (t/\tau_0)^{1-\alpha}$ when $0 < \alpha < 1$ for the autocorrelation function. The power-law behaviour found in the structural fluctuations suggests that the irradiation field in an HVEM can provide a means to explore non-equilibrium open systems. The present results also suggest that our irradiated compound is a self-organized-criticality system. However, in order to understand this behaviour better, direct measurement of the lifetime distribution of clusters in the power form $\tau^{-\alpha}$ will be necessary. Various aspects of transient atomic clusters and their dynamic structural changes are currently under investigation (for example Watanabe *et al.* 2003).

ACKNOWLEDGEMENTS

We are grateful to Dr P. R. Okamoto, Dr T. Matsukawa and Dr K. Arakawa for helpful discussions. This work was partially supported by Kazato Foundation, The Japanese Ministry of Education, Grant-in-aid for Scientific Research (No. 15560569), and the US Department of Energy, Office of Science, under contract W-31-109-Eng-38.

REFERENCES

- ANGELL, C. A., NAGAI, K. L., MCKENNA, G. B., McMILLAN, P. F., and MARTIN, S. W., 2000, *J. appl. Phys.*, **88**, 3113.
- BAK, P., TANG, C., and WIESENFELD, K., 1987, *Phys. Rev. Lett.*, **50**, 381; 1988, *Phys. Rev. A*, **38**, 364.
- BANERJEE, S., KULKARI, U. D., and URBAN, K., 1989, *Acta metall.*, **37**, 35.
- BANERJEE, S., URBAN, K., and WILKENS, M., 1984, *Acta metall.*, **32**, 299.
- CROSS, M. C., and HOHENBERG, P. C., 1993, *Rev. mod. Phys.*, **65**, 851.
- DAW, M. S., and BASKES, M. I., 1984, *Phys. Rev. B*, **29**, 6443.
- DEBENEDETTI, P. G., and STILLINGER, F. H., 2001, *Nature*, **410**, 259.
- DUTTA, P., and HORN, P. M., 1981, *Rev. mod. Phys.*, **53**, 497.
- HOGGE, F. N., and BOBBERT, P. A., 1997, *Physica B*, **239**, 223.
- ISHIZUKA, K., and UYEDA, N., 1977, *Acta crystallogr. A*, **33**, 740.
- KADANOFF, L. P., 1966, *Physics*, **2**, 263.
- KAUZMANN, W., 1948, *Chem. Rev.*, **43**, 219.
- KOIKE, T., WATANABE, S., HOSHINO, M., SUDA, T., OHNUKI, S., TAKAHASHI, H., and LAM, N. Q., 2002, *Mater. Trans.*, **43**, 1716.
- KRAMER, E. M., and LOBKOVSKY, A. E., 1996, *Phys. Rev. E*, **53**, 1465.
- LAM, N. Q., OKAMOTO, P. R., and LI, M., 1997, *J. nucl. Mater.*, **251**, 89.
- MANDELBROT, B., 1982, *The Fractal Geometry of Nature* (San Francisco, California: Freeman).
- MORI, H., FUJITA, H., TENDO, M., and FUJITA, H., 1984, *Scripta metall.*, **18**, 783.
- NAYAK, S. K., RAMASWAMY, R., and CHAKRAVARTY, C., 1995, *Phys. Rev. Lett.*, **74**, 4181.
- OKAMOTO, P. R., LAM, N. Q., and REHN, L. E., 1999, *Solid St. Phys.*, **52**, 1.
- SABOCHICK, M. J., and LAM, N. Q., 1991, *Mater. Res. Soc. Symp.*, **201**, 387.
- SETHNA, J. P., DAHMEN, K. A., and MYERS, C. R., 2001, *Nature*, **410**, 242.
- SHIBROT, T., and MUZZIO, F. J., 2001, *Nature*, **410**, 251.
- STILLINGER, F. H., 1995, *Science*, **267**, 1935.
- TAKAI, Y., KAWASAKI, T., KIMURA, Y., IKUTA, T., and SIMIZU, R., 2001, *Phys. Rev. Lett.*, **87**, 106105.
- VAN DER ZIEL, A., 1950, *Physica*, **16**, 359.
- WALGRAEF, D., 1997, *Spatio-temporal Pattern Formation: With Examples from Physics, Chemistry, and Materials Science* (New York: Springer).
- WATANABE, S., HOSHINO, M., KOIKE, T., SUDA, T., OHNUKI, S., TAKAHASHI, H., and LAM, N. Q., 2003, *J. Electron Microsc.*, **52**, 33.
- WATANABE, S., KOIKE, T., SUDA, T., OHNUKI, S., TAKAHASHI, H., and LAM, N. Q., 2001, *Phil. Mag. Lett.*, **81**, 789.
- WILLIAMS, D. B., and CARTER, C. B., 1992, *Transmission Electron Microscopy* (New York: Plenum), pp. 328, 465.